Optimizing the fluorescent yield in two-photon laser scanning microscopy with dispersion compensation

Jeffrey J. Field,[1,*] Ramón Carriles,[1,6] Kraig E. Sheetz,[1,7] Eric V. Chandler,[1] Erich E. Hoover,[1] Shane E. Tillo,[2] Thom E. Hughes,[2] Anne W. Sylvester,[3] David Kleinfeld,[4] and Jeff A. Squier[1]

[1]*Center for Microintegrated Optics for Advanced Bioimaging and Control, and Department of Physics, Colorado School of Mines, 1523 Illinois Street, Golden, CO 80401, USA*
[2]*Department of Cell Biology and Neuroscience, Montana State University, Bozeman, Montana 59717, USA*
[3]*Department of Molecular Biology, University of Wyoming, Laramie, Wyoming 82071, USA*
[4]*Department of Physics, Graduate Program in Neurosciences, and Center for Neural Circuits and Behavior, University of California at San Diego, La Jolla, CA 92093, USA*
[6]*Present address: Department of Photonics, Centro de Investigaciones en Optica, A. C., León, 37150 A.P. 1-948, México*
[7]*Present address: Department of Physics and Nuclear Engineering, United States Military Academy, West Point, New York 10996, USA*
*jjfield@mines.edu

Abstract: A challenge for nonlinear imaging in living tissue is to maximize the total fluorescent yield from each fluorophore. We investigated the emission rates of three fluorophores—rhodamine B, a red fluorescent protein, and CdSe quantum dots—while manipulating the phase of the laser excitation pulse at the focus. In all cases a transform-limited pulse maximized the total yield to insure the highest signal-to-noise ratio. Further, we find evidence of fluorescence antibleaching in quantum dot samples.

©2010 Optical Society of America

OCIS codes: (170.0180) Microscopy; (180.4315) Nonlinear microscopy; (180.2520) Fluorescence microscopy; (320.5540) Pulse shaping.

References and links

1. W. Denk, J. H. Strickler, and W. W. Webb, "Two-photon laser scanning fluorescence microscopy," Science **248**(4951), 73–76 (1990).
2. F. Helmchen, and W. Denk, "Deep tissue two-photon microscopy," Nat. Methods **2**(12), 932–940 (2005).
3. E. J. Sánchez, L. Novotny, G. R. Holtom, and X. S. Xie, "Room-temperature fluorescence imaging and spectroscopy of single molecules by two-photon excitation," J. Phys. Chem. A **101**(38), 7019–7023 (1997).
4. G. H. Patterson, and D. W. Piston, "Photobleaching in two-photon excitation microscopy," Biophys. J. **78**(4), 2159–2162 (2000).
5. A. Diaspro, G. Chirico, C. Usai, P. Ramoino, and J. Dobrucki, in Handbook of Biological Confocal Microscopy, 3rd. Ed., (ed. James B. Pawley) Ch. 39, 690–702 (Springer Science + Business Media, 2006).
6. N. Ji, J. C. Magee, and E. Betzig, "High-speed, low-photodamage nonlinear imaging using passive pulse splitters," Nat. Methods **5**(2), 197–202 (2008).
7. P. Xi, Y. Andegeko, L. R. Weisel, V. V. Lozovoy, and M. Dantus, "Greater signal, increased depth, and less photobleaching in two-photon microscopy with 10 fs pulses," Opt. Commun. **281**(7), 1841–1849 (2008).
8. G. Donnert, C. Eggeling, and S. W. Hell, "Major signal increase in fluorescence microscopy through dark-state relaxation," Nat. Methods **4**(1), 81–86 (2007).
9. H. Kawano, Y. Nabekawa, A. Suda, Y. Oishi, H. Mizuno, A. Miyawaki, and K. Midorikawa, "Attenuation of photobleaching in two-photon excitation fluorescence from green fluorescent protein with shaped excitation pulses," Biochem. Biophys. Res. Commun. **311**(3), 592–596 (2003).
10. J. J. Field, C. G. Durfee 3rd, J. A. Squier, and S. Kane, "Quartic-phase-limited grism-based ultrashort pulse shaper," Opt. Lett. **32**(21), 3101–3103 (2007).
11. R. Carriles, K. E. Sheetz, E. E. Hoover, J. A. Squier, and V. Barzda, "Simultaneous multifocal, multiphoton, photon counting microscopy," Opt. Express **16**(14), 10364–10371 (2008).
12. R. Trebino, Frequency-Resolved Optical Gating: The Measurement of Ultrashort Laser Pulses, (Kluwer Academic Publishers, Norwell, MA, 2000).
13. W. Amir, T. A. Planchon, C. G. Durfee, J. A. Squier, P. Gabolde, R. Trebino, and M. Müller, "Simultaneous visualization of spatial and chromatic aberrations by two-dimensional Fourier transform spectral interferometry," Opt. Lett. **31**(19), 2927–2929 (2006).

14. D. J. Kane, G. Rodriguez, A. J. Taylor, and T. S. Clement, "Simultaneous measurement of two ultrashort laser pulses from a single spectrogram in a single shot," J. Opt. Soc. Am. B **14**(4), 935–943 (1997).
15. D. J. Kane, "Principal components generalized projections: a review [Invited]," J. Opt. Soc. Am. B **25**(6), A120–A132 (2008).
16. D. N. Fittinghoff, A. C. Millard, J. A. Squier, and M. Müller, "Frequency-resolved optical gating measurement of ultrashort pulses passing through a high numerical aperture objective," IEEE J. Quantum Electron. **35**(4), 479–486 (1999).
17. M. Drobizhev, S. Tillo, N. S. Makarov, T. E. Hughes, and A. Rebane, "Absolute two-photon absorption spectra and two-photon brightness of orange and red fluorescent proteins," J. Phys. Chem. B **113**(4), 855–859 (2009).
18. A. Shavel, N. Gaponik, and A. Eychmüller, "Covalent linking of CdTe nanocrystals to amino-functionalized surfaces," ChemPhysChem **6**(3), 449–451 (2005).
19. C. R. Dietrich, M. A. D. N. Perera, M. D. Yandeau-Nelson, R. B. Meeley, B. J. Nikolau, and P. S. Schnable, "Characterization of two GL8 paralogs reveals that the 3-ketoacyl reductase component of fatty acid elongase is essential for maize (Zea mays L.) development," Plant J. **42**(6), 844–861 (2005).
20. A. Mohanty, Y. Yang, A. Luo, A. W. Sylvester, and D. Jackson, "Methods for generation and analysis of fluorescent protein-tagged maize lines," Methods Mol. Biol. **526**, 71–89 (2009).
21. C. Xu, and W. W. Webb, "Measurement of two-photon excitation cross sections of molecular fluorophores with data from 690 to 1050 nm," J. Opt. Soc. Am. B **13**(3), 481–491 (1996).
22. A. J. Berglund, "Nonexponential statistics of fluorescence photobleaching," J. Chem. Phys. **121**(7), 2899–2903 (2004).
23. W. G. J. H. M. van Sark, P. L. T. M. Frederix, D. J. Van den Heuvel, H. C. Gerritsen, A. A. Bol, J. N. J. van Lingen, C. de Mello Donegá, and A. Meijerink, "Photooxidation and photobleaching of single CdSe/ZnS quantum dots probed by room-temperature time-resolved spectroscopy," J. Phys. Chem. B **105**(35), 8281–8284 (2001).
24. C. Bardeen, V. Yakovlev, J. Squier, K. R. Wilson, S. D. Carpenter, and P. M. Weber, "Effect of pulse shape on the efficiency of multiphoton processes: implications for biological microscopy," J. Biomed. Opt. **4**(3), 362–367 (1999).
25. D. Meshulach, D. Yelin, and Y. Silberberg, "Real-time spatial-spectral interference measurements of ultrashort optical pulses," J. Opt. Soc. Am. B **14**(8), 2095–2098 (1997).
26. P. Bowlan, P. Gabolde, A. Shreenath, K. McGresham, R. Trebino, and S. Akturk, "Crossed-beam spectral interferometry: a simple, high-spectral-resolution method for completely characterizing complex ultrashort pulses in real time," Opt. Express **14**(24), 11892–11900 (2006).
27. J. J. Field, T. A. Planchon, W. Amir, C. G. Durfee, and J. A. Squier, "Characterization of a high efficiency, ultrashort pulse shaper incorporating a reflective 4096-element spatial light modulator," Opt. Commun. **278**(2), 368–376 (2007).
28. M. Müller, J. Squier, R. Wolleschensky, U. Simon, and G. J. Brakenhoff, "Dispersion pre-compensation of 15 femtosecond optical pulses for high-numerical-aperture objectives," J. Microsc. **191**(2), 141–150 (1998).

1. Introduction

Two-photon laser scanning microscopy (TPLSM) with fluorescent indicators is a unique and critical means to probe structure and function in biological systems. This approach excites only molecules at the focus of the objective [1,2] and thus does not lead to photobleaching of fluorophores away from the region of interest. Despite this advantage, the bleaching rates within the focal excitation region are significantly increased as compared to confocal microscopy [3,4]. This is a serious problem that limits the acquisition of data, particularly in *in vivo* functional and structural studies. Yet the mechanisms that cause the increase in photobleaching are not fully understood [5]. Improvements to photostability in two-photon excited fluorescence (TPEF) microscopy have been attempted by manipulation of the femtosecond excitation pulses in terms of their energy [4,6,7], repetition rate [6,8], and shape [7,9]. Past work investigating the pulse shape dependence considered decreases in the bleaching rate as a function of pulse shape and pulse energy [9]. Here we examine bleaching rates and yields in the power-limited case, which is often encountered in deep-tissue imaging [2].

We study three biologically relevant fluorophores, *i.e.*, Rhodamine B isothiocyanate-Dextran (RhB-ITC), Tag red fluorescent protein (TagRFP), and CdSe quantum dots (QDs), in aqueous environments. We ask, first, can we define the spatial and temporal characteristics of the laser pulse at the focus of a high numerical aperture objective? Toward this goal we use a grism-based ultrashort pulse shaper [10] in combination with a dual focal, two-photon imaging system [11] to systematically manipulate the excitation pulse intensity and phase at the focus of high numerical aperture objectives, and introduce a new variant of frequency-resolved optical-gating (FROG) [12] to characterize the pulse shape at the focus. Second, how

does the fluorescent yield depend on the temporal pulse shapes at the focus of the excitation laser? Photon counting enables us to quantify the number of emitted photons per pixel dwell time in the presence of bleaching, *i.e.*, the number of emitted photons during the exposure time. Lastly, we consider the application of our methods toward imaging living plant cells that express monomeric red fluorescent protein (mRFP).

2. Experimental methods

2.1 Apparatus

To characterize photobleaching as a function of spectral dispersion, we used a titanium-doped sapphire (Ti:Al$_2$O$_3$) extended cavity oscillator with a 21.7 MHz repetition rate and central wavelength of 808 nm as the excitation source. Two spectral bandwidths of 19 nm and 40 nm (measured at the full-width at half-maximum (FWHM) of the spectral intensity) were used for these studies, for reasons described in the following subsection. Using the laser spectrum, we calculated transform-limited pulse durations of 51 fs and 20 fs respectively for these bandwidths. Average powers in the sample plane of the microscope were measured to be 11.2–11.7(± 0.1) mW for the pulse shapes used.

The microscope used in this study was a multifocal system with two foci in the sample plane [11]. To achieve multiple foci, shaped pulses from the grism pulse shaper were split using a polarizing beam splitter (PBS), with a λ/2 waveplate to control the power ratio between the two arms. The two beams were then retro-reflected back through the PBS by inserting a λ/4 waveplate in each arm to rotate the polarization of each pulse by 90 degrees after double-passing, thereby transmitting both pulses to the microscope scan optics. Since the input pulse was split with a single PBS, the two beams transmitted to the scan optics are collinear and orthogonally polarized.

Measurement of photobleaching data was performed in a modified commercial microscope body (IX-71, Olympus) with a photomultiplier tube (PMT; Hamamatsu R7400) measuring two-photon fluorescence in the epi-direction. All measurements were performed in photon-counting mode. Laser pulses were focused with a 0.75 NA/40x objective (UPlanFLN, Olympus). Fluorescence was detected through a 600–655 nm bandpass filter (FMF005, ThorLabs). A 1-mm-thick BG-39 filter was inserted prior to the bandpass filter for additional attenuation of back-scattered excitation light.

2.2 Spectral dispersion compensation and pulse shaping

To accurately synthesize the desired pulse shape at the focus of a multi-element, high NA objective, the operating regime must be carefully determined. In multiphoton microscopy, spatial aberrations are ultimately coupled to temporal distortions. The extent of this coupling can be precisely determined by using two-dimensional spectral interferometry (2DSI) [13]. Specifically, one can extract the impact of the spatial distortions on pulse duration. Previous measurements of the coupling between spatial and temporal distortion were used to establish important imaging boundaries. For example, 2DSI measurements on a 1.25 NA Zeiss objective indicated that for pulse durations greater than 50 fs, spherical aberration is dominant, and while the focus broadens spatially as a result of this distortion, the impact on pulse duration is negligible. Conversely, for pulse durations on the order of 15 fs, the chromatic aberration is dominant, and will result in broadening the pulse duration to approximately 25 fs [13]. In the case of these very short pulses, distortions are a complex mix of radially varying aberrations. Presently, it is not possible to compensate for these effects. For longer pulse durations (>50 fs), however, the effects of spatial distortions for this optical system are effectively decoupled from time, meaning that both the spatial aberrations and the spectral dispersion can be readily compensated.

Being able to precisely measure this "break point" in the optics (that is the pulse duration where spatial and temporal aberrations effectively decouple) enabled us to design this study to operate in a regime where the pulse shaper can fully compensate for the temporal pulse broadening. By limiting pulse durations to 20–50 fs or longer, we ensured that the targeted

pulse shape was effectively produced at the focus and was not distorted by spatial or chromatic aberrations of the scan optics or excitation objective. This was further reinforced by our ability to directly extract the pulse shape at the full NA of the objective. Thus, while previous studies have investigated the effect of temporal pulse shape on photobleaching rates, we study these rates in biologically relevant fluorophores and with bandwidths that allow for transform limited pulses to be synthesized at the focal plane of the microscope, without the complication of chromatic aberrations which cannot be compensated. Direct measurements of temporal pulse shapes at the excitation plane of our microscope are correlated to photobleaching rates and fluorescence yield for the first time to our knowledge.

Spectral dispersion of excitation pulses was removed at the sample plane with a grism-based femtosecond pulse shaper [10]. The unique properties of the grism pulse shaper allowed for the removal of all second-order dispersion (SOD), or equivalently, group delay dispersion (GDD), and third-order dispersion (TOD) by adjusting passive controls of the device. This reserved the dynamic range of a liquid crystal spatial light modulator (LC SLM; Boulder Nonlinear Systems, Lafayette, CO) for programmable control of the spectral phase and removal of higher-order dispersion (HOD). This pulse shaping system introduces negligible spatial chirp for the bandwidths considered here [10].

We investigated four different pulse shapes: (1) the input (INP) pulse, which was transform-limited at the input to the microscope; (2) the third-order-limited (TOL) pulse, in which all second-order dispersion was removed at the image plane; (3) the fourth-order-limited (FOL) pulse, for which all second- and third-order dispersion were removed at the image plane; and (4) the objective (OBJ) pulse, which was optimized by a genetic algorithm to obtain transform limited pulses at the image plane.

To synthesize the INP pulse, the intensity of second-harmonic generation (SHG) from a β-BaB_2O_4 crystal was maximized at the output of the grism pulse shaper. Because the intensity of SHG is maximal for a transform limited pulse [7], we used an evolutionary strategy (ES) with the intensity of SHG as the feedback parameter to find transform limited pulses. The variable space was the collection of spectral masks that may be written to the LC SLM. Alternatively, we have spectrally resolved the SHG signal and optimized the area under its intensity envelope. It was found that both optimization parameters resulted in transform-limited (TL) pulses at the β-BaB_2O_4 crystal plane.

To find the TOL and FOL pulses, the excitation pulse was focused into a sample of Rhodamine 6G in water (Rh6G-H_2O). Since the sample was allowed to freely diffuse, we measured the TPEF from a supply of unbleached fluorophores diffusing into the focal volume, and therefore detected no photobleaching from this sample. To remove second-order dispersion (GDD) from the pulse, we adjusted the passive controls of the grism pulse shaper to remove only GDD (see Ref. 10). As in the case of SHG, TPEF is maximized by transform limited pulses, as long as the excitation power is kept below the saturation level of the dye. By maximizing the TPEF signal in this way, we removed all the GDD from the pulse. Next we adjusted the passive controls of the pulse shaper to remove both TOD and GDD from the pulse. Again, by maximizing the TPEF signal from a non-bleaching sample of Rhodamine 6G, we removed all GDD and TOD from the pulse.

Finally, to find the OBJ pulse, the ES was again employed to iterate on the spectral phase of the pulse to maximize the TPEF signal from the Rh6G-H_2O sample. In this way, HOD was removed from the pulse, and we synthesize a pulse that is as close to TL as possible in the focal plane of the objective.

To collect bleaching data, the field-of-view of each sample was first imaged to ensure that the sample was homogeneous [Fig. 1(a)]; we used the longest-duration pulse for this purpose to minimize bleaching. We then excited a specific location within the field-of-view for several seconds and collected the fluorescence. Seven spots were irradiated for each of the four pulse shapes [Fig. 1(b)], then averaged to obtain a photobleaching curve [Fig. 1(d)]. After bleaching, the sample was imaged once more to ensure that no sample drift occurred during the exposure that could cause fluorophore replenishment in the excitation volume [Fig. 1(b)].
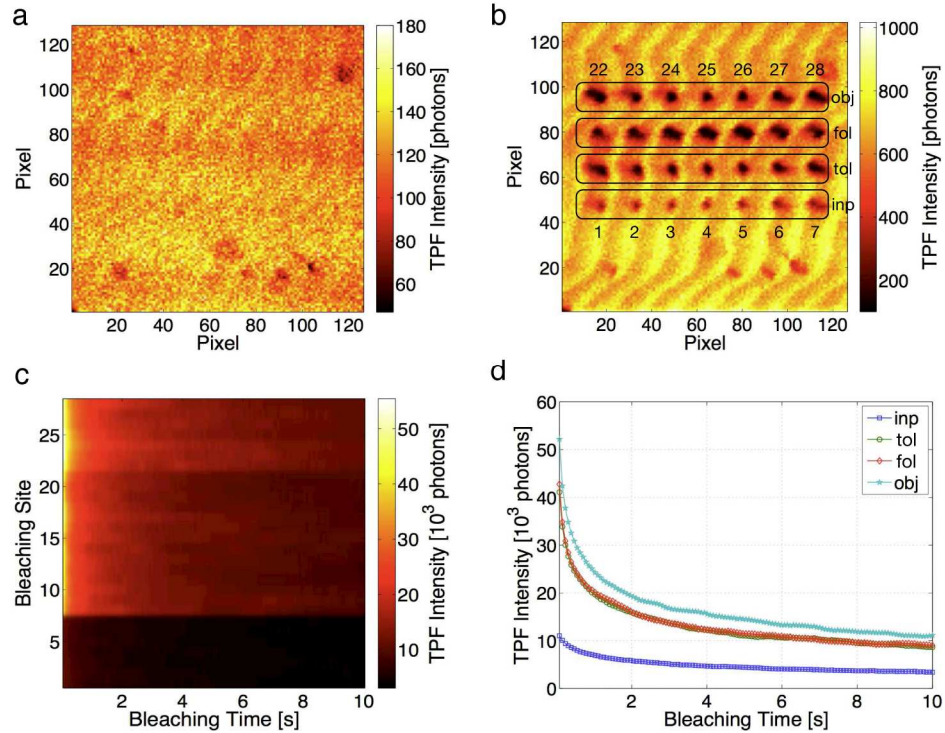
Fig. 1. Method for quantifying photobleaching in the non-scanning mode. (a) Image of a RhB-ITC sample prior to bleaching, taken with the INP pulse. (b) Image of the sample after photobleaching measurements, imaged with the OBJ pulse. Note the increase in photons/pixel with the OBJ pulse. (c) Bleaching data is stored in a two-dimensional matrix during the bleaching measurement. (d) Averaged photon-counted photobleaching curves for each pulse shape. Note that this figure is intended to be an example only, and data obtained in this figure are not part of the experimental results discussed below.

Data was also acquired in scanning mode for a square area 45 µm on a side. Each image was scanned at one frame per second for one hundred seconds, corresponding to a pixel dwell time of 61 µs for the 128x128-pixel images collected. The first image of the series was viewed immediately after data acquisition to ensure homogeneity of the fluorophore distribution in the FOV. The average photon count in the FOV for each image of the series was computed and plotted as a function of time. Each data point in this mode represents the average over all 16,384 pixels contained in an image.

2.3 Type-II Blind FROG pulse characterization in the focal plane

Frequency-resolved optical-gating (FROG) provides a means to characterize femtosecond pulses. A spectrally resolved signal is generated by two pulses that overlap in both space and time in a nonlinear medium, and is recorded as a function of delay between the pulses [12]. In our system, the two pulses overlap in the sample plane and are orthogonally polarized [11]. Even though the pulses at each foci accumulate different amounts of dispersion, the intensity envelope and phase of each pulse may be simultaneously extracted through blind deconvolution [12,14,15] of a single FROG measurement in the focal plane of the objective.

By overlapping the pulses from the multifocal system spatially and temporally inside a KDP crystal with type-II phase matching at the sample plane, we measured a background free second-harmonic generation (SHG) FROG trace at the focus of the excitation objective. Collinear type-II SHG FROG at the full numerical aperture of an excitation objective has been reported [16]. Our pulse characterization technique was different from that in Ref. 16 in that each pulse experienced a different amount of spectral dispersion in the multifocal system due

to the additional optics needed for divergence correction on one pulse. This means that the temporal electric fields of each pulse were different, whereas a typical collinear SHG FROG trace would be carried out with identical pulses [16]. When this measurement is performed with different pulses it is known as Blind FROG, indicating that neither electric field is known and must be found from a single measurement [12]. By making a slight modification to the standard principle components generalized projections algorithm (PCGPA) [15] for retrieving the amplitude and phase of an ultrashort pulse from a FROG trace, we were able to simultaneously extract both pulses from a single Blind FROG measurement. Since we knew that one pulse always passed more glass than the other, we were able to distinguish which pulse was used for the bleaching measurements, thereby directly characterizing the electric field of the excitation pulse in the sample plane.
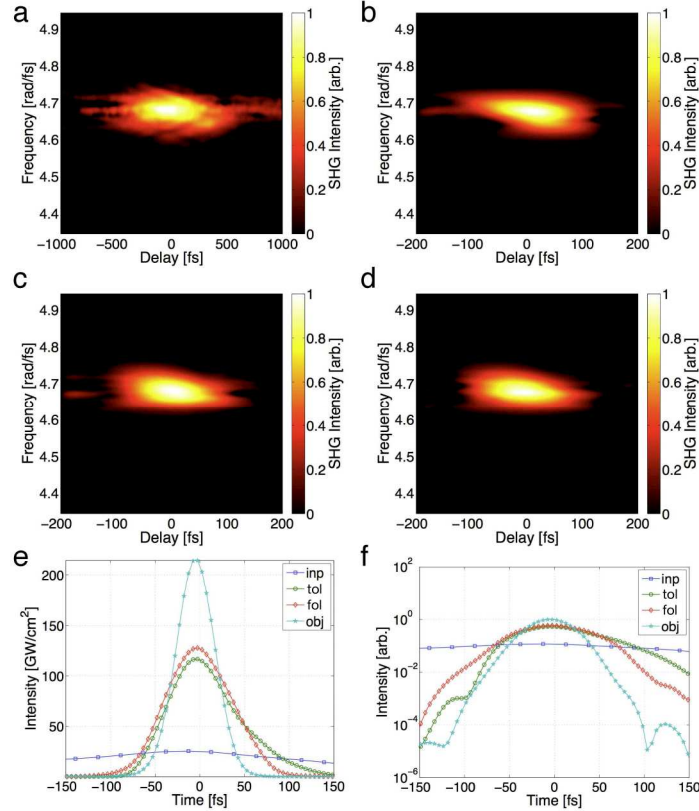

Fig. 2. Measured pulse shapes in the focal plane of the excitation objective. Blind FROG traces for (a) INP, (b) TOL, (c) FOL, and (d) OBJ pulses obtained in focus. Extracted pulse shapes with calculated peak intensities (see text) are shown on a (e) linear and (f) logarithmic scale. FROG errors for the reconstructed traces were (a) 0.019, (b) 0.019, (c) 0.012, and (d) 0.014, each on a 80x80 point grid.

Blind FROG traces measured in the focal plane of the objective for all four pulse shapes are shown in Figs. 2(a)–2(d), with corresponding extracted pulse shapes displayed in Fig. 2(e) and Fig. 2(f). Peak intensities were calculated for each pulse according to the relation

$$I_{peak} = g \, \frac{P_{ave}}{A} = \frac{g_p}{\tau \, f} \, \frac{P_{ave}}{\pi \, r_0^2} \tag{1.1}$$

where g is the second-order temporal coherence of the pulse, P_{ave} is the average power in the beam, A is the lateral area of the point-spread function in focus, g_p is the shape factor of the pulse, τ is the pulse duration at the full-width at half-maximum (FWHM) of the intensity

envelope, f is the repetition rate of the oscillator, and r_0 is the radius of the focal spot. By using the bleached image [*e.g.*, Fig. 1(b)] to estimate the localization area, we combine measurements of the pulse profile, laser repetition rate, and average power in the sample plane to determine the peak intensity for each pulse. Note that while the temporal pulse shape is taken into account in Eq. (1.1), the spatial profile of the beam is assumed to be a top-hat shape.

2.4 Preparation of photobleaching samples

Three fluorophores were investigated for *in vitro* bleaching measurements. Each sample was prepared in a chemical environment intended to inhibit diffusion while mimicking a physiological environment.

The Rhodamine B samples were composed of Rhodamine-B-isothiocyanate-Dextran (RhB-ITC, Sigma Aldrich) suspended in an Agarose gel. The RhB-ITC was dissolved in a Na-HEPES buffer solution (150 mM, pH = 7.4) to a concentration of 37.2 µM. Agarose (SeaPrep Agarose, Lonza Rockland, Inc.) was then added to the RhB-ITC/Na-HEPES solution (90 mg of Agarose powder to 50 mL of solution) and the mixture was heated to approximately 100 C until the Agarose powder was completely dissolved. The heated mixture was then allowed to cool to room temperature, and a 10 µL drop of the fluorescent gel was placed between two cover slips for imaging. The slides were placed in a refrigerator at approximately 5 C for several hours to allow the Agarose gel to completely harden prior to data collection.

Two samples of TagRFP were prepared for these experiments. The first sample was prepared in a similar fashion to the RhB-ITC samples. A slight change was made to the procedure, as heating of the fluorescent proteins can cause denaturing and thus lead to erroneous concentrations. TagRFP samples were received in an imidazole buffer solution (pH = 8.0) at unknown concentrations. Spectrophotometric measurements were performed using the peak absorption extinction coefficient of 85,600 $M^{-1}cm^{-1}$, determined from the Strickler-Berg equation [17], to determine the concentration of TagRFP in the provided samples. The sample used to prepare bleaching slides was found to be 4.95 µM. Instead of adding the TagRFP directly the Na-HEPES buffer solution before heating, Agarose was dissolved into the buffer solution by the method described above. Once the mixture cooled to 35 C, the TagRFP/Imidazole solution and Na-HEPES/Agarose solution were mixed 1:1, and a 10 µL drop was then placed between two cover slips, and cooled to 5 C to allow the Agarose gel to fully harden.

The second TagRFP sample was made using phosphate buffered saline (PhBS, 10 mM, pH = 7.4) and porcine gelatin. First, 2 g of porcine gelatin was dissolved into 100 mL of boiling PhBS solution, then allowed to cool to room temperature. The TagRFP and PhBS/gelatin solution were mixed 1:1, and then 10 µL of the TagRFP gel was placed on a cover slip. While the solution was cooling, 1.5 µL of 10% v/v gluteraldehyde/H_2O was added to the TagRFP gelatin to crosslink the proteins. After the gluteraldehyde was allowed to diffuse through the gel and the sample had cooled, another cover slip was placed on top, and the TagRFP perfusate gel was then sealed between the two cover slips using nail polish. Again, samples were cooled to 5 C to allow the porcine gelatin to harden.

Quantum dot (QD) samples were prepared with commercial CdSe nanocrystals (Invitrogen, QDot ITK carboxyl quantum dots, 625 conjugate). The QDs have a CdSe core with a ZnS shell, and carboxylic-acid terminated surface groups attached to the outer shell. The QDs were shipped at a concentration of 8 µM in a 50 mM borate buffer solution at pH = 9.0. To prepare immobilized samples of QDs, we covalently bonded the carboxylic-acid groups attached to the shell of the QDs to an amino-functionalized glass slide (aminopropylsilane microarray slides, Thermo Scientific) using an established procedure [18]. To complete the reaction, two solutions were prepared. The first was made by dissolving 24 mg of 1-Ethyl-3-[3-dimethylaminopropyl]carbodiimide Hydrochloride (EDC) and 27.2 mg of N-hydroxysulfosuccinimide (Sulfo-NHS) into 5 mL of deionized water. This solution serves as the catalyst for the covalent bonding reaction. The second solution prepared was a buffer

solution of 2-[morpholino]ethanesulfonic (MES) at 6.25 µM. The purpose of this buffer solution was simply to match the pH of the EDC/Sulfo-NHS catalyst solution, which increases the bonding efficiency during the reaction. As the pH of these solutions does not affect the fluorescent properties of the final samples, their pH was not recorded. The reaction was performed by placing a functionalized glass slide into a bath of the buffer solution in a Petri dish. Next, 50 µL of the QDs solution was added to the bath. Finally, 600 µL of the EDC/Sulfo-NHS solution was added to the bath, which was continuously stirred for 15 minutes. Afterwards, the slide was removed and washed with water, acetone, and toluene, before being dried by a nitrogen jet. Samples were then stored at 5 C for several days before imaging.

Maize plants used for *in vivo* studies were genetically modified to express the GLOSSY8 (GL8) protein tagged with mRFP using protocols described elsewhere [19,20]. Briefly, to ensure native gene expression the full length genomic sequence of the gene encoding GL8, including regulatory regions 3 kilobases (kb) upstream and 2 kb downstream of the coding sequence were PCR amplified to include the coding sequence for mRFP at the start codon, cloned into Gateway vectors (Invitrogen) and prepared for maize transformation at the Plant Transformation Facility at Iowa State University.

3. Results

We observe that both the fluorescence emission and bleaching rates increase as the duration of excitation pulses is decreased for both molecular dyes [Fig. 3(a), 3(b)]. We tabulated both the rate of TPEF bleaching and the total number of photons for constant incident power versus the second-order temporal coherence (*g*) of the pulse at the focus (Table 1). This metric, defined as:

$$g \equiv \frac{\int_{-\infty}^{\infty} dt \, f \, I^2(t)}{\left[\int_{-\infty}^{\infty} dt \, f \, I(t) \right]^2} \qquad (1.2)$$

where *f* is again the repetition rate of the laser, and *I(t)* is the temporal intensity, accurately characterizes the pulse width and shape [21]. We note that the bleaching curves do not exhibit single-exponential decay, as expected due to the non-uniform spatial illumination intensity [22]. Bleaching rates were determined by fitting a sum of three exponentials to the fluorescence curves, and using the analytical representation of the decay curves to find the time needed to decay by a set amount (Table 1). The slight increase in bleaching rate between the FOL and OBJ pulses for the RhB-ITC sample illustrates the general trend in the RhB-ITC data where higher order correction is difficult to distinguish.

We observe an increase in yield as the beam approaches the transform limit at the focus, indicating we maintain pulse intensities below the saturation intensities of each fluorophore. Moreover, we find no deviation from quadratic behavior for TPEF intensity versus average power in aqueous non-bleaching samples (data not shown).
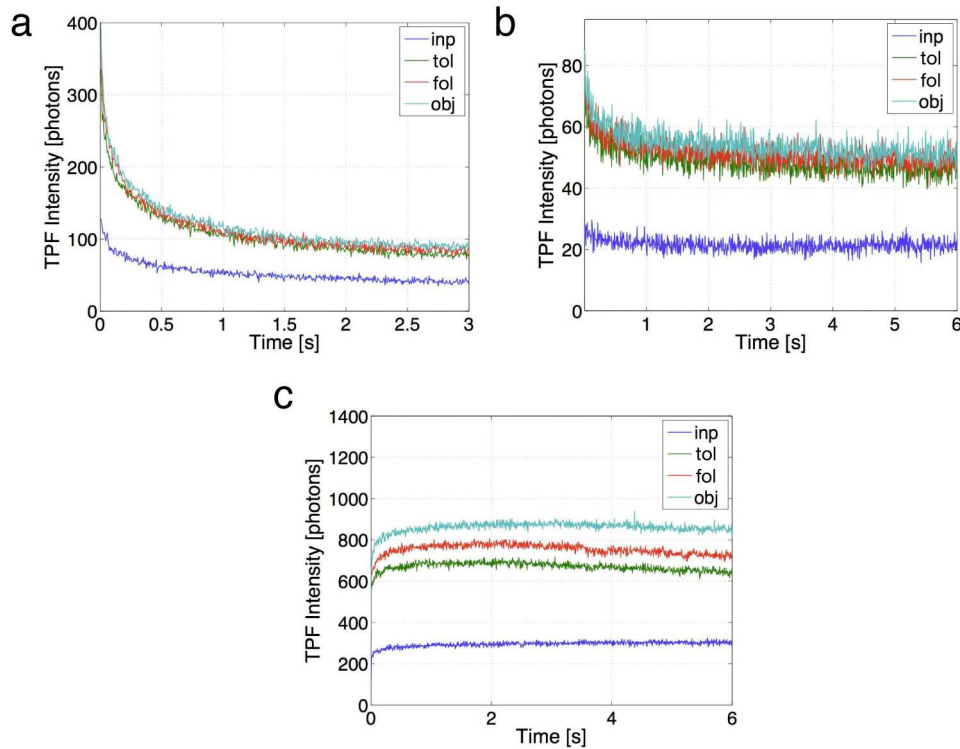
Fig. 3. Photobleaching data corresponding to the pulse shapes displayed in Fig. 2. Bleaching curves for (a) RhB-ITC, (b) TagRFP, crosslinked in porcine gelatin, and (c) QD samples.

Table 1. Photobleaching rates and fluorescence yield in all three fluorophores and corresponding measurements of the second-order temporal coherence obtained from Blind FROG

Excitation Pulse		Bleaching Rate [s^{-1}]			TPEF Yield [10^3 photons]		
Shape	g [x10^3]	RhB-ITC[a]	TagRFP[b]	QDs[c]	RhB-ITC	TagRFP	QDs
INP	66.7	1.32	0.364	0.174	45.120	22.001	301.771
TOL	323	1.91	2.31	0.338	91.366	49.797	684.667
FOL	354	2.34	3.88	0.232	100.145	52.570	770.328
OBJ	597	2.08	4.74	0.184	107.205	55.245	879.652
Bleaching rates are measured at [a]50%, [b]85%, and [c]110% of the initial intensity values.							

Unlike the two organic molecules, quantum dots show an initial increase in fluorescence – antibleaching – followed by slow decay in fluorescence [Fig. 3(c)]. The rates for quantum dot antibleaching were determined as the inverse of the time needed for the fluorescence signal to reach 110% of its initial intensity. The rates were again calculated by fitting the fluorescence curves to a functional form, in this case a bi-exponential decay that was inverted to represent an increase in fluorescence as a function of excitation time. In contrast to antibleaching, the slow decay of the fluorescence was expected in light of the high photostability of quantum dots compared to other fluorophores [23]. Lastly, fluorescent yield increases as the second-

order temporal coherence [cf. Eq. (1.2)] of the pulse increased for all fluorophores, as expected from theoretical considerations (Table 1) [5,21].

As the duration of excitation pulses is decreased, stretching due to spectral dispersion becomes more pronounced. While GDD is the main cause of pulse stretching in the data shown in Fig. 3, TOD and HOD play crucial roles in shorter excitation pulses [21,24]. To illustrate this, we increased the bandwidth of our oscillator from approximately 19 nm to 40 nm, corresponding to transform limited pulse durations of 51 fs and 20 fs respectively. According to previous studies, chromatic aberration is still negligible for the 20 fs pulses [13]. Using a variation of spectral interferometry called SEA TADPOLE [25–27], we have previously characterized the amount of GDD in our microscope to be approximately 5700 fs^2. This amount of GDD stretches the 51 fs pulse to 286 fs, while stretching the 20 fs pulse to 694 fs. This example illustrates that as more bandwidth is added to the pulse, dispersion has a larger impact on pulse duration. We therefore expected that by increasing the bandwidth of the Ti:Al$_2$O$_3$ oscillator, removal of TOD and HOD would have a more drastic affect on the fluorescence yield and bleaching rate, as had been observed in previous studies [28].

Bleaching curves for the expanded bandwidth pulses for RhB-ITC and TagRFP samples are shown in Fig. 4, where Fig. 4(a) and Fig. 4(b) show bleaching in the non-scanning mode, while Fig. 4(c) and Fig. 4(d) show bleaching in the scanning mode. As expected, we observed a greater increase in the fluorescence yield with correction of HOD as compared to the longer excitation pulses, for which the majority of the increase in fluorescence is found by correcting GDD [21,24].
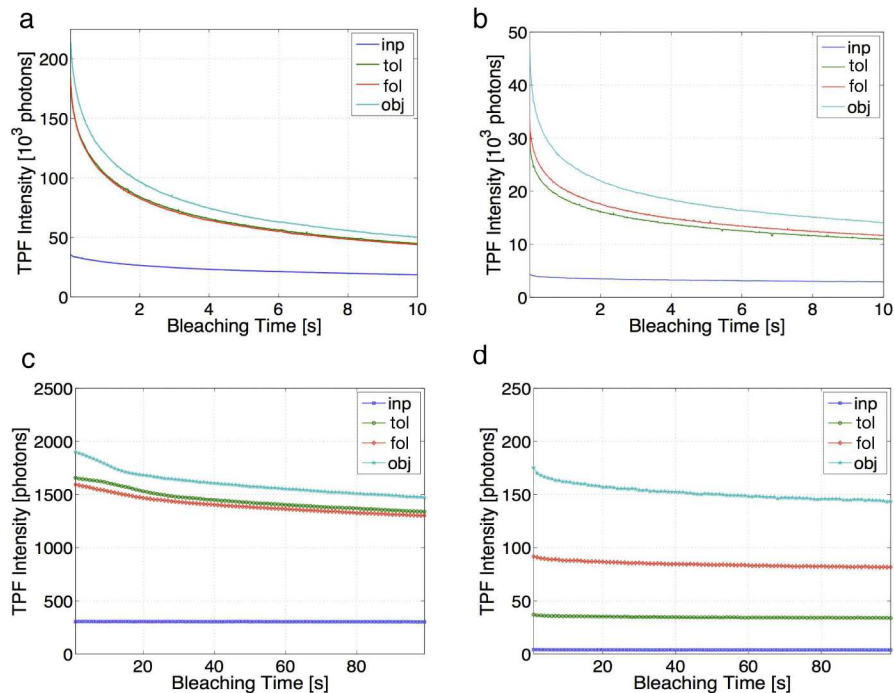

Fig. 4. Photobleaching curves with broadband femtosecond pulses. Bleaching in non-scanning mode for (a) Rhodamine B and (b) TagRFP in agarose, and scanning mode for (c) Rhodamine B and (d) TagRFP. Second order correction improves the number of emitted photons in all cases. The distinction between TOL and FOL pulses yields little or no improvement for (a) & (c), and is essentially within the signal to noise of the measurement.

Our *in vitro* results demonstrate that laser pulses that are transform limited at the focus significantly improve the efficiency of two-photon driven fluorescence for the fluorophores and wavelengths used in this study (Table 1), despite the concurrent increase in photobleaching rates, resulting in an improved signal-to-noise ratio (SNR) during the duration

of the measurement. In order for the instantaneous fluorescence from the OBJ pulse to fall below that of the INP pulse, thereby decreasing SNR from TL pulses, we found that bleaching times on the order of one hundred seconds were required. Since no real-world TPEF microscopy experiment approaches dwell times on the order of one hundred seconds, it is safe to assume that the signal from the OBJ pulse will always result in better SNR. Moreover, as previous reports have indicated [4], one can simply decrease the average excitation power to obtain the minimum acceptable SNR to minimize bleaching further.

To test responses in the complex environment of a biological sample, epidermal cells of maize plants that were genetically modified to express mRFP were used to test for fluorescence photobleaching *in vivo*. The transform limited pulse yields improved contrast and enhancement of cellular features [Fig. 5(a), 5(b)]. This improvement persists as a function of time [Fig. 5(d), 5(e)]. An average of the fluorescence across the entire sample [Fig. 5(f)] shows that the yields with a transform pulse at the focus results in an ~5-times improvement in the total fluorescent yield, and display bleaching dynamics similar to those found in our *in vitro* studies.
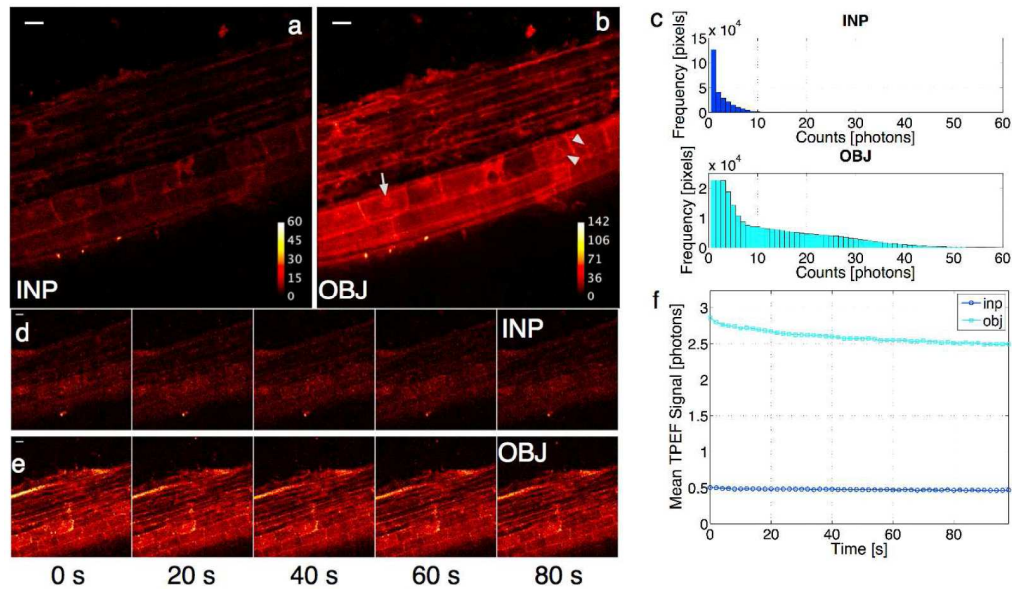

Fig. 5. Improvement of TPEF signal by shortening excitation pulse in epidermal cells of a maize plant expressing the GL8 protein tagged with mRFP. Images were taken with (a) INP and (b) OBJ pulses respectively. In the OBJ image, the arrow points to mRFP concentration near the nucleus, while the arrowheads indicate cytoplasmic strands in the cell. Note that the only post-processing of these images is the false color intensity map, and that the contour numbers in the calibration bar represent photon count. The improvement in imaging with a TL pulse at the sample plane is clear from the histogram of the photon counts in each image shown in (c). Scanning photobleaching tests were performed *in vivo* using the INP and OBJ pulses, as shown in (d) and (e) respectively. Each image was acquired in 2 seconds (0.5 Hz, 256x256-pixel) for 50 consecutive images. The mean photon count as a function of imaging time was calculated, and is displayed in (f). The photobleaching rates and intensities follow the same pattern as that observed in homogeneous TagRFP samples. Scale bars are 10 µm.

4. Conclusions

We have directly characterized the shape of the excitation pulse in the focal plane of a two-photon microscope (Fig. 2) and correlated this data with photobleaching of two fluorophores, Rhodamine B and TagRFP (Figs. 1,3 and 4). We find that excitation with a transform-limited pulse significantly increases the efficiency of excitation and thus improves the signal-to-noise ratio of two-photon imaging compared with the signal-to-noise ratio obtained using an

uncompensated pulse (Table 1). Thus an increase in the bleaching rate of the dye as a result of the increased efficiency is exceeded by the increase in fluorescent yield.

An unanticipated result is that correction of phase beyond third order dispersion has a measurable impact on the excitation efficiency for pulses as long as 50 fs in duration. This is of practical importance as most commercial Ti:Al$_2$O$_3$ lasers sold for biological imaging purposes have durations in the range of 50-100 fs. Moreover, the improvement in the two photon fluorescence signal scales approximately as the inverse of pulse duration for Rhodamine B while the fluorescence measured from the TagRFP sample increases more dramatically with higher-order correction (Fig. 4).

A pragmatic point concerns the throughput of the pulse shaping device. The intensity of the fluorescence signal varies as the square of the average excitation power [21], yet is linearly proportional to the second order coherence. As an example, if one uses a pulse shaper with 50% throughput, the fluorescence intensity will fall to 25% of the original level, assuming the same pulse duration. Thus it is important to ensure that the gain in fluorescence from the reduction of the pulse duration will offset the loss in fluorescence due to throughput losses in the pulse shaping apparatus.

Acknowledgements